Two-Hole and Four-Hole Bound States in a $t-J$ Ladder at half-filling

Weihong Zheng* and C.J. Hamer†

School of Physics, The University of New South Wales, Sydney, NSW 2052, Australia.

(Dated: February 1, 2008)

The two-hole excitation spectrum of the $t-J$ ladder at half-filling is studied using linked-cluster series expansion methods. A rich spectrum of bound states emerges, particularly at small t/J. Their dispersion relations and coherence lengths are computed, along with the threshold behaviour as the bound states merge into the continuum. A class of 4-hole bound states is also studied, leading to the conclusion that phase separation occurs for $t/J \lesssim 0.5$, in agreement with other studies.

I. INTRODUCTION

Ladder models of magnetic and electronic systems, such as the Heisenberg, $t-J$ and Hubbard ladders, have attracted great interest in recent years[1,2], on both theoretical and experimental grounds. The ladders provide a "half-way house" between one-dimensional and two-dimensional systems, and display new and interesting behaviour in their own right. The spin-$\frac{1}{2}$ Heisenberg ladder, for instance, forms a magnetically disordered *spin liquid*, with a finite spin gap[1]. Experimentally, two-leg $S=\frac{1}{2}$ ladders are found in some cuprates like $SrCu_2O_3$[3]; while the ladder material $Sr_{14-x}Ca_xCu_{24}O_4$ has recently been found to show superconductivity under high pressure[4].

In this paper we study two-hole bound states which occur in the $t-J$ ladder at half-filling, using a newly developed linked-cluster series expansion method for 2-particle states[5]. A rich spectrum of multiparticle bound states will be revealed. The properties of 2-particle states, such as their dispersion relations, coherence lengths and exclusive structure factors, can provide much important information about the dynamics of the model at hand, providing a stringent test of any analytical model of the system. These properties are also amenable to experimental test, via neutron scattering or other techniques. In the case of the Heisenberg ladder, for instance, a model[6,7] based on triplet excitations of a ground state consisting of singlet dimers on each rung of the ladder[8,9,10] provides a reasonable qualitative description of the numerical results for both 1- and 2-particle excitations, not only in the dimer limit, but even for the isotropic case. Ideally, one would like to achieve a similar convergence between analytical theory and numerical 'experiment' for the case of the $t-J$ ladder.

The basic properties of the $t-J$ ladder have been explored by exact diagonalizations[11,12,13,14,15,16,17], the density renormalization group[18,19,20,21], quantum Monte Carlo simulation[22], and series expansion techniques[23,24], as well as approximate analytic theories[19,20,25,26,27,28]. The Hamiltonian of the $t-J$ ladder is

$$\begin{aligned} H = \quad & J\sum_{i,a}(\mathbf{S}_{i,a}\cdot\mathbf{S}_{i+1,a}-\frac{1}{4}n_{i,a}n_{i+1,a}) + J_\perp\sum_i(\mathbf{S}_{i,1}\cdot\mathbf{S}_{i,2}-\frac{1}{4}n_{i,1}n_{i,2}) \\ & -t\sum_{i,a,\sigma}P(c^\dagger_{i,a,\sigma}c_{i+1,a,\sigma}+H.c.)P - t_\perp\sum_{i,\sigma}P(c^\dagger_{i,1,\sigma}c_{i,2,\sigma}+H.c.)P \end{aligned} \tag{1}$$

where i labels sites along each chain, σ (=↑ or ↓) and a (=1,2) are spin and leg indices, and P is a projection

operator which excludes doubly occupied sites. The constants J, t are exchange and hopping parameters on each chain, while $J_\perp$, $t_\perp$ are coupling parameters between the two chains, i.e. on the rungs of the ladder.

The scenario is then as follows[13].

Starting from the half-filled case, and in the dimer limit of strong interchain coupling $J_\perp, t_\perp$, the ground state consists of spin singlet dimers on each rung, as in the Heisenberg ladder. The lowest spin excitation is a triplet excitation on one rung, propagating via the coupling between the rungs. There are also hole excitations with spin-$\frac{1}{2}$, which carry both spin and charge. The lowest 2-hole excitation consists of a singlet hole pair on one rung, which again develops into a band by propagation along the ladder. Relative to the 2-hole ground state, this then corresponds to a gapless band of particle-hole charge excitations: thus the system is said to be in a Luther-Emery C1S0 phase (1 gapless charge mode, 0 gapless spin modes). The spin gap evolves discontinuously away from half-filling[13], because there is a triplet particle-hole excitation of lower energy than the triplet magnon state referred to above.

A phase diagram in the J/t versus electron density n plane, for the case of isotropic couplings, has been proposed by Poilblanc *et al.*[12] and by Müller and Rice[16]. For $J/t \gtrsim 2$, phase separation is predicted to occur[21]. For $J/t \lesssim 2$ and low to moderate doping the system is in a C1S0 phase, and crosses to a C1S1 phase (i.e. the spin gap vanishes) for higher doping. For small J/t and low doping Müller and Rice[16] also find ferromagnetic (Nagaoka) and C2S2 phases. Superconducting pairing correlations occur away from half-filling[11,14,25].

Jurecka and Brenig[28] have recently constructed an analytic model of the 2-hole bound states on the $t-J$ ladder, starting from a rung dimer ground state as discussed above, and including both 1-hole pseudofermion elementary excitations and 2-hole singlet excitations on a single rung. They find a low-lying $S=0$ bound state in good agreement with exact diagonalization calculations, but the triplet gap is underestimated as the isotropic limit is approached.

The outline of the paper as follows: in Sect. II we briefly describe our series expansion method, while Section III present results for pairs of 'even parity' and 'odd parity' excitations respectively, A rich and complex spectrum of bound states is revealed. Sect. IV discusses 4-hole bound states formed from two hole-pairs, each on a single rung, and this allows some discussion of phase separation. Sect. V give a summary and discussion. All the bound states discussed in this paper involve identical 'single particle' components; bound states of non-identical components will be treated in a separate paper.

II. METHOD

We employ a "rung basis", in which the 2nd and 4th terms in (1) form the unperturbed Hamiltonian H_0, and the remaining terms are treated perturbatively. That is, the Hamiltonian (1) is rewritten as

$$H = H_0 + xV \tag{2}$$

where

$$\begin{aligned} H_0 &= J_\perp[\sum_i(\mathbf{S}_{i,1}\cdot\mathbf{S}_{i,2} - \frac{1}{4}n_{i,1}n_{i,2}) \\ &\quad -y_1\sum_{i,\sigma}P(c^\dagger_{i,1,\sigma}c_{i,2,\sigma} + H.c.)P] \end{aligned} \tag{3}$$

$$\begin{aligned} V &= J_\perp[\sum_{i,a}(\mathbf{S}_{i,a}\cdot\mathbf{S}_{i+1,a} - \frac{1}{4}n_{i,a}n_{i+1,a}) \\ &\quad -y_2\sum_{i,a,\sigma}P(c^\dagger_{i,a,\sigma}c_{i+1,a,\sigma} + H.c.)P] \end{aligned} \tag{4}$$

and $x = J/J_\perp$, $y_1 = t_\perp/J_\perp$, and $y_2 = t/J$.

The eigenstates of H_0 are direct products constructed from the nine possible rung states, which are listed in Table I for easy reference. In the half-filled case, the lowest energy rung state is a spin-singlet state $(|\uparrow\downarrow\rangle - |\downarrow\uparrow\rangle)/\sqrt{2}$. The ground state of the unperturbed Hamiltonian, at half-filling, is then a direct product of these spin-singlet

states on each rung. The lowest spin excitation, at half-filling, consists of a spin-triplet excitation on one rung, which propagates coherently along the ladder. One and two-hole charge excitations are created by removing one or two electrons from a rung state and allowing these to propagate, via the t-hopping term. In our previous work[23], we have studied the 1-hole properties, and the properties of 2-holes sitting on the same rung. The study of the dynamic properties of 2-holes sitting on different rungs is much more complicated: these have been studied by Jurecka and Brenig[28] and by Troyer, Tsunetsugu and Rice[13].

Recently, we have developed strong-coupling series expansion methods to study two-particle spectra of quantum lattice models[29]. These methods allow us to precisely determine the low-lying excitation spectra of the models at hand, including all two-particle bound/antibound states, at least for small x. In this paper, we apply this new technique to study the dynamic properties of 2-holes in the $t-J$ ladder.

As discussed in our previous paper[29], to compute the two-particle properties, we first calculate an effective Hamiltonian in the two-particle sector

$$E_2(\mathbf{i},\mathbf{j};\mathbf{k},\mathbf{l}) = \langle \mathbf{k},\mathbf{l}|H^{\rm eff}|\mathbf{i},\mathbf{j}\rangle \ , \tag{5}$$

and then calculate the irreducible two-particle matrix element

$$\begin{aligned}\Delta_2(\mathbf{i},\mathbf{j};\mathbf{k},\mathbf{l}) \ = \ & E_2(\mathbf{i},\mathbf{j};\mathbf{k},\mathbf{l}) - E_0(\delta_{\mathbf{i},\mathbf{k}}\delta_{\mathbf{j},\mathbf{l}} + \delta_{\mathbf{i},\mathbf{l}}\delta_{\mathbf{j},\mathbf{k}}) \\ & -\Delta_1(\mathbf{i},\mathbf{k})\delta_{\mathbf{j},\mathbf{l}} - \Delta_1(\mathbf{i},\mathbf{l})\delta_{\mathbf{j},\mathbf{k}} \\ & -\Delta_1(\mathbf{j},\mathbf{k})\delta_{\mathbf{i},\mathbf{l}} - \Delta_1(\mathbf{j},\mathbf{l})\delta_{\mathbf{i},\mathbf{k}} \ , \end{aligned} \tag{6}$$

where δ refers to a Kronecker delta function and Δ_1 is the one-particle irreducible matrix element. Once the effective two-particle Hamiltonian is known, we still have to solve the Schrödinger equation. The two particle continuum is delimited by the maximum (minimum) energy of two single particle excitations whose combined momentum is the center of mass momentum. There may be multiple solutions to the Schrödinger equation above or below the two-particle continuum. Those solutions with energy below the bottom edge of the continuum are the bound states, while those with energy higher than the upper edge of the continuum are the antibound states. The binding energy is defined as the energy difference between the lower edge of the continuum and the energy of the bound state, while the antibinding energy is defined as the energy difference between the upper edge of continuum and the energy of an antibound state.

To compute the perturbation series we choose values for the free parameters y_1, y_2, and derive expansions in powers of x. Series have been computed to order x^{11}. The calculations involve (trivial) 1-dimensional clusters up to 12 rungs, and are limited to this order by computer memory constraints. To avoid excessive data here we mainly consider the case that $y_1 = y_2$. The series for the energies of the lowest singlet bound states S_1 and S_2 and triplet bound state T_1 (and also the lower edge of the continuum) at band maximum $k = \pi$ for $y_1 = y_2 = 0.1$ are given in Table II. Other series are available on request.

In the small x limit our strong coupling series are highly accurate and we can find all details of various two-particle bound (and antibound) states. The overall 2-particle spectrum is much richer than that obtained in previous studies. Several singlet and triplet bound/antibound states are found. The number of bound states depends on the coupling constants as well as the wavevector.

Previous numerical studies[13,28] on small lattices have concentrated on the coupling $y_1 = 1/3$, $y_2 = 10/3$, and $t = t_\perp$, and found one singlet bound state in the even parity channel. Unfortunately, our series expansions do not converge well at this coupling, so we can not make a direct comparison. In order to check the correctness of our results, we also did some finite lattice calculations on small systems, and find very good agreement for the lowest energy bound state. The finite lattice calculations on small systems certainly are not accurate enough, how-

ever, to see other bound states sitting very close to the lower edge of the continuum.

III. TWO-HOLE BOUND STATES

A. Even-parity channel

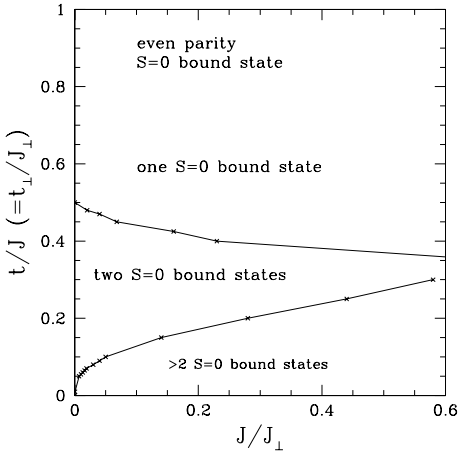

FIG. 1: A diagram for the number of singlet bound states for the even-parity channel in the plane of $t/J(= t_\perp/J_\perp)$ and $J/J_\perp$.

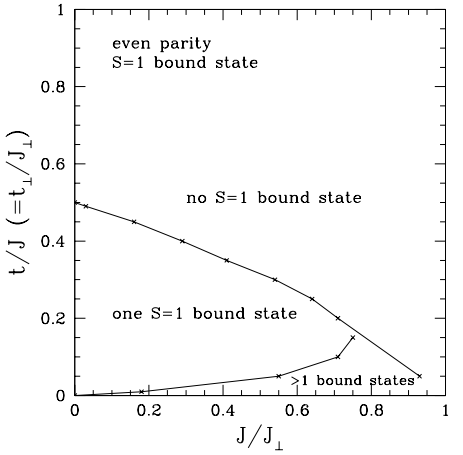

FIG. 2: A diagram for the number of triplet bound states for the even-parity channel in the plane of $t/J(= t_\perp/J_\perp)$ and $J/J_\perp$.

Among the nine eigenstates for the unperturbed Hamiltonian H_0 on each rung, there are the following two spin-$\frac{1}{2}$ electron-hole bonding states[29]

$$\frac{1}{\sqrt{2}}(|\,0\uparrow\rangle + |\uparrow 0\rangle) \tag{7}$$

$$\frac{1}{\sqrt{2}}(|\,0\downarrow\rangle + |\downarrow 0\rangle)\ ,$$

which have 'even parity' with respect to reflection across the ladder. The eigenenergy for these two states is $-t_\perp$. In this section, we discuss the bound states formed from two of these excitations.

We find that the number of bound states and antibound states depends strongly on $J/J_\perp$ and $t/J(= t_\perp/J_\perp)$. Ignoring the antibound states, Fig. 1 show the number of singlet ($S = 0$) bound states in the plane of $t/J(= t_\perp/J_\perp)$ and $J/J_\perp$. We can see that for large t/J ($t/J \gtrsim 0.5$) there is only one singlet bound state, while around $t/J \simeq 0.3$, there is a region where there are two singlet bound states, and for smaller t/J and $J/J_\perp > 0$, there is a region where there are more than 2 singlet bound states. In this region, the number of bound state increases as $J/J_\perp$ increases. Note that all these are in addition to the singlet state consisting of a pair of holes on the same rung.

Fig. 2 shows the number of triplet ($S = 1$) bound states in the same plane. We can see that for large t/J ($t/J \gtrsim 0.5$) there are no triplet bound states, whereas around $t/J \simeq 0.2$ and small $J/J_\perp$, there is a region where there is only one triplet bound state, and for smaller t/J and $J/J_\perp > 0$, there is a region where there are multiple triplet bound states. The existence of these multiple bound states has not been noted before, to our knowledge. Note also that the triplet bound states appear to vanish as the isotropic case $J/J_\perp$ is approached.

Now let us look at a particular case $t/J = t_\perp/J_\perp = 0.1$ (i.e. small hopping parameters) and $J/J_\perp = 0.2$. The two-particle excitation spectrum is shown in Fig. 3. One can see from these graphs that there are three singlet bound states (S_1, S_2 and S_3) and one triplet bound state (T_1) below the continuum, and two triplet antibound states (T_2 and T_3) above the continuum, in addition to the state S_0 corresponding to a hole pair on a single rung. All the dispersion bands are very flat, as expected

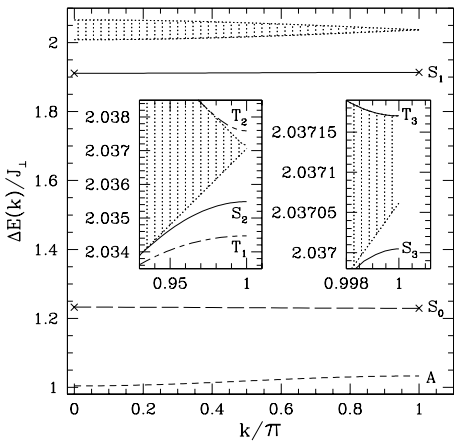

FIG. 3: The excitation spectrum for the even parity channel with $t/J = t_\perp/J_\perp = 0.1$ and $J/J_\perp = 0.2$. Beside the two-particle continuum (gray shaded), there are three singlet bound states (S_1, S_2 and S_3) and one triplet bound state (T_1) below the continuum, and two triplet antibound states (T_2 and T_3) above the continuum. The insets enlarge the region near $k = \pi$ so we can see S_2, S_3, T_1 and T_2, but the antibound state T_3 is still indistinguishable from the continuum. Curve A is the dispersion of the one-hole bonding state, while curve S_0 is the dispersion of two-holes sitting on the same rung. The cross points are the results of exact diagonalization for the 8-rung finite lattice with periodic boundary condition.

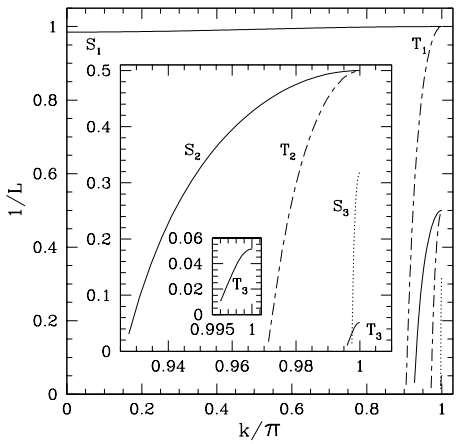

FIG. 4: The inverse of the coherence length $1/L$ versus momentum k for three singlets (S_1, S_2 and S_3), one triplet (T_1) bound state, and two triplet (T_2 and T_3) antibound states for the even parity channel at $t/J = t_\perp/J_\perp = 0.1$ and $J/J_\perp = 0.2$. The inset enlarges the region near $k = \pi$.

for small hopping parameters. The singlet bound state S_1 exists for the whole range of momenta (its coherence length L is finite also for the whole range of momenta), while other bound/antibound states exist only in a limited range of momenta near $k = \pi$. Figure 4 shows the inverse of the coherence length $1/L$ versus momentum k for these various bound states. At $k = \pi$, the coherence length L for S_1 and T_1 is 1, for S_2 and T_2, it is about 2, S_3 has coherence length L about 3, while for T_3 the coherence length L is very large, about 20 (its antibinding energy at $k = \pi$ is very small, $E_b/J_\perp = 8.9\times10^{-8}$, so T_3 is indistinguishable from the two-particle continuum in Fig. 3). This means that the formation of bound/antibound states S_1, T_1 , S_2, T_2, S_3 is largely due to the interaction of two bonding rungs separated by distances 1, 1, 2, 2, and 3 respectively, while the formation of T_3 is much more complicated. For comparison, also shown in Fig. 3 is the dispersion for the one-hole bonding state, and the dispersion of two-holes sitting on the same rung[23]: here two holes sitting on the same rung have lower energy.

To check the correctness of our series calculations, we also performed an exact diagonalization for a finite lattice of 8 rungs with periodic boundary condition for this set of parameters. The results for $k = 0, \pi$ are also shown in Fig. 3. There is remarkable agreement for the state S_1, but the finite lattice calculation is not accurate enough to give the other bound states sitting very close to the continuum.

We now study the behaviour as a function of the coupling ratio $J/J_\perp$, fixing $t/J = t_\perp/J_\perp = 0.1$ and $k = \pi$. The binding/antibinding energies E_b and the inverse of the coherence length $1/L$ versus $J/J_\perp$ are shown in Figs. 5 and 6. In the small J limit, there are two singlet bound states S_1 and S_2 (with coherence lengths 1 and 2, respectively), one triplet bound state T_1 (coherence length 1), and one triplet antibound state T_2 (coherence length 2). As J increases, more and more singlet and triplet bound states appear: we find that the singlet/triplet bound/antibound states S_3, S_4, S_5 and T_3 appear at

$J/J_\perp$ about 0.0480, 0.39, 0.55 and 0.180 respectively. To find out the behaviour near the threshold, we plot in Fig. 7 the square root of the binding energy $(E_b/J_\perp)^{1/2}$ and the inverse of the coherence length $1/L$ versus $J/J_\perp$ for singlet bound state S_3. We can see that near threshold, the curves are nearly straight lines, which implies that near threshold $E_b \propto (x - x_c)^2$ and $L \propto (x - x_c)^{-1}$, corresponding to "threshold indices" 2 and -1, respectively, where $x = J/J_\perp$. For a fixed value of $J/J_\perp$, the threshold behaviour as a function of momentum is $E_b \propto (k - k_c)^2$, $L \propto (k - k_c)^{-1}$. We expect similar behaviour for other bound/antibound states (but see Sect. IV).

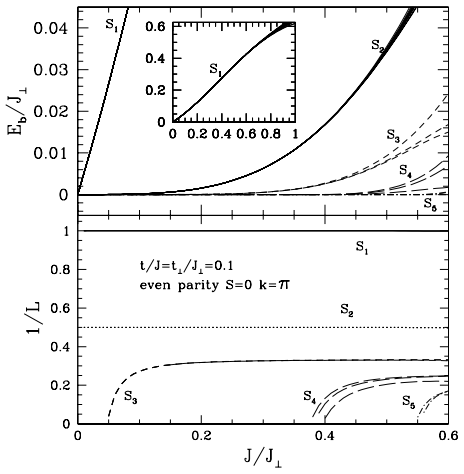

FIG. 5: The binding energy E_b and the inverse of the coherence length $1/L$ versus $J/J_\perp$ for the singlet bound states in the even parity channel at $t/J = t_\perp/J_\perp = 0.1$ and $k = \pi$. For the binding energy of S_1 and S_2, the results of several different integrated differential approximants to the series are shown, while for other curves, the results of the three highest orders are plotted.

Next we consider the case $t/J = t_\perp/J_\perp = 1$ (stronger hopping terms) and $J/J_\perp = 0.2$. The two-particle excitation spectrum and the inverse of the coherence length $1/L$ versus momentum k are shown in Figs. 8 and 9. Here there is only one singlet bound state S_1 below the continuum, and one triplet antibound state (T_1) above it. Both S_1 and T_1 exist only in a limited range of momenta near $k = \pi$, and their coherence lengths L at $k = \pi$ are about 1. As comparison, also shown in Fig. 8 is the dispersion for the one-hole bonding state, and the dispersion of two-holes sitting on the same rung[23], S_0. In this case the state S_0 actually lies above the state S_1, and even above the 2-particle continuum.

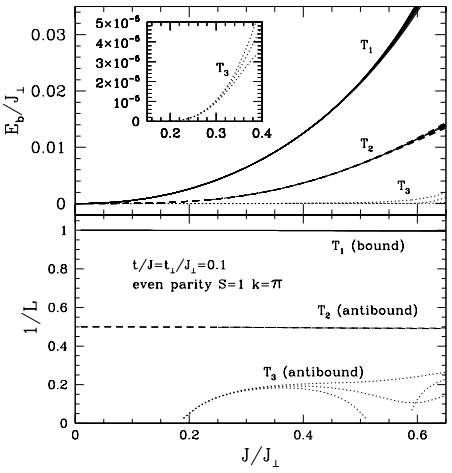

FIG. 6: The binding/antibinding energy E_b and the inverse of the coherence length $1/L$ versus $J/J_\perp$ for triplet bound/antibound states in the even parity channel at $t/J = t_\perp/J_\perp = 0.1$ and $k = \pi$. For the binding/antibinding energy of T_1 and T_2, the results of several different integrated differential approximants to the series are shown, while for other curves, the results of the three highest orders are plotted.

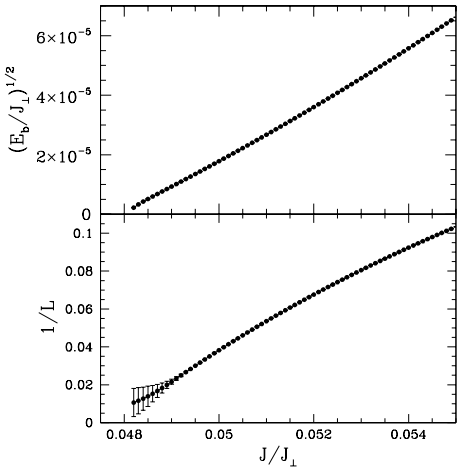

FIG. 7: The square root of the binding energy $(E_b/J_\perp)^{1/2}$ and the inverse of the coherence length $1/L$ versus $J/J_\perp$ for the singlet bound state S_3 in the even parity channel at $t/J = t_\perp/J_\perp = 0.1$ and $k = \pi$.

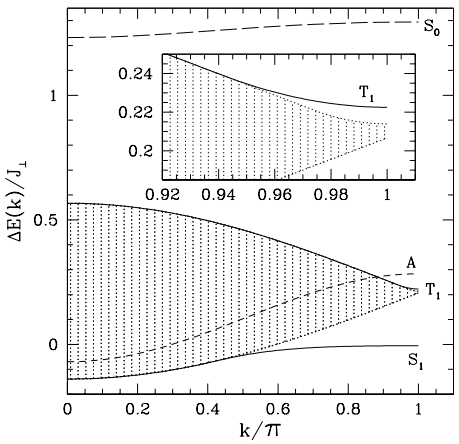

FIG. 8: The excitation spectrum for the even parity channel with $t/J = t_\perp/J_\perp = 1$ and $J/J_\perp = 0.2$. Beside the two-particle continuum (gray shaded), there is one singlet bound state (S_1) below the continuum, and one triplet antibound state (T_1) above the continuum. The insets enlarges the region near $k = \pi$ to show T_1 above the continuum. The curve labeled A is the dispersion of one hole, while the curve labeled S_0 is the dispersion of two holes on the same rung.

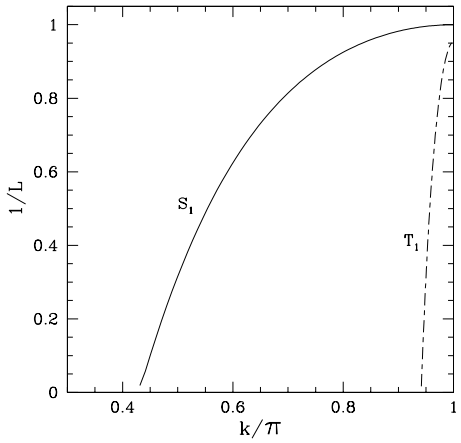

FIG. 9: The inverse of the coherence length $1/L$ versus momentum k for the singlet S_1 and one triplet antibound state T_1 in the even parity channel at $t/J = t_\perp/J_\perp = 1$ and $J/J_\perp = 0.2$.

the coherence length $1/L$ versus $J/J_\perp$ are shown in Fig. 10. One can see that the singlet bound state S_1 and the triplet antibound state T_1 exist in the small J limit, but as J increases, no more new bound/antibound states appear.

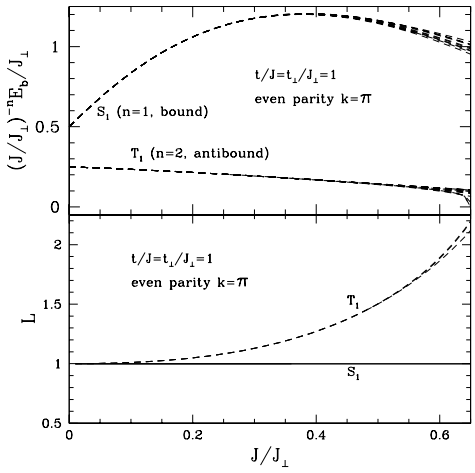

FIG. 10: The (anti)-binding energy E_b and the inverse of the coherence length $1/L$ versus $J/J_\perp$ for singlet/triplet (anti)-bound states in the even parity channel with $t/J = t_\perp/J_\perp = 1$ and $k = \pi$. For the (anti)-binding energy, the results of several different integrated differential approximants to the series are shown, while for the inverse of the coherence length $1/L$, the results of the three highest orders are plotted.

Sometimes a bound state can appear in the regions near both $k = 0$ and $k = \pi$, but not at intermediate momenta. For example for $t/J = t_\perp/J_\perp = 0.425$, the binding energy and coherence length L for $J/J_\perp = 0.025$, 0.05 and 0.075 are shown in Fig. 11. For very small $J/J_\perp$ (0.025 and 0.05 in the figure), the singlet bound state exists over the whole range of momenta, but for larger $J/J_\perp$ (0.075 in the figure), this singlet bound state only exists in the regions near both $k = 0$ and $k = \pi$, but not in the intermediate regions of momentum.

As already seen above, the lowest energy 2-hole bound state may correspond to a pair of holes on the same rung (S_0), or two holes on different rungs (S_1), depending on the parameters $t/J(= t_\perp/J_\perp)$ and $J/J_\perp$. The boundary between these two situations is shown in Fig. 12: we will refer back to this diagram later on.

B. Odd-parity channel

Among nine rung eigenstates for the unperturbed Hamiltonian H_0 in each rung, there are the following two

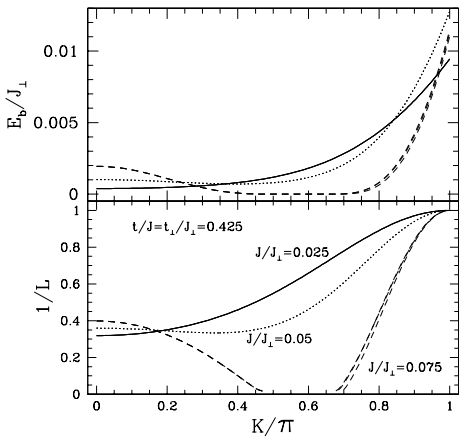

FIG. 11: The binding energy E_b and the inverse of the coherence length $1/L$ versus k for the first singlet bound state in the even parity channel at $t/J = t_\perp/J_\perp = 0.425$ and $J/J_\perp = 0.025$ (solid lines), 0.05 (dotted lines), and 0.07 (dashed lines). The results of the three highest orders are plotted. Note that for these couplings there is a second singlet bound state and a triplet bound state near $k = \pi$, which are not plotted.

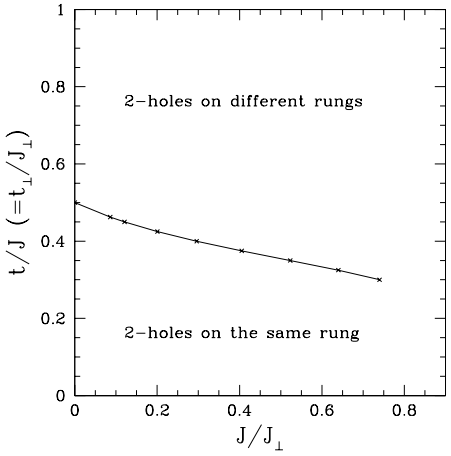

FIG. 12: Boundary between different configurations of the lowest-lying 2-hole bound state.

spin-$\frac{1}{2}$ odd-parity electron-hole antibonding states

$$\frac{1}{\sqrt{2}}(|\,0\downarrow\rangle - |\downarrow 0\rangle)$$
$$\frac{1}{\sqrt{2}}(|\,0\uparrow\rangle - |\uparrow 0\rangle) \qquad (8)$$

The eigen energy for these two states is $t_\perp$. In this section, we discuss bound states of these two 1-particle excitations.

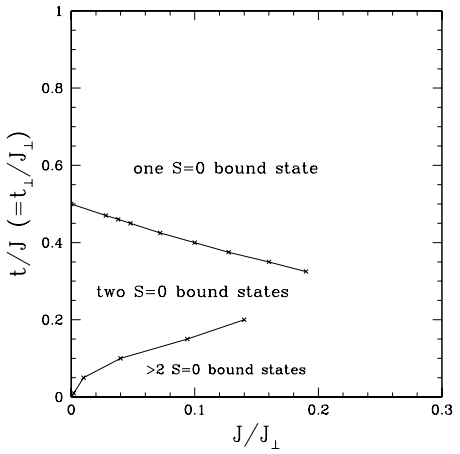

FIG. 13: The number of singlet bound states in the odd-parity channel in the plane of $t/J(= t_\perp/J_\perp)$ and $J/J_\perp$.

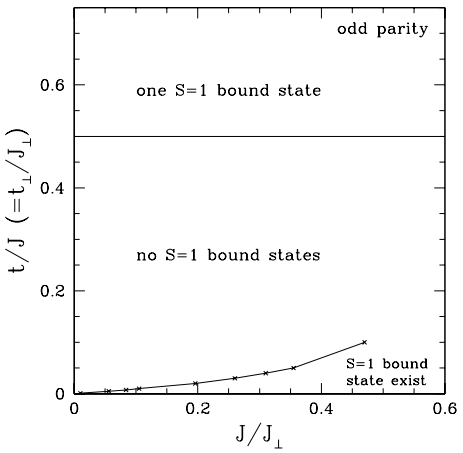

FIG. 14: The number of triplet bound states in the odd-parity channel in the plane of $t/J(= t_\perp/J_\perp)$ and $J/J_\perp$.

As for the case of even parity, the number of bound states and antibound states depends on $J/J_\perp$ and $t/J(= t_\perp/J_\perp)$. Fig. 13 shows the diagram for the number of singlet ($S = 0$) bound states, where we can see that for large t/J ($t/J \gtrsim 0.5$) there is only one singlet bound state, while around $t/J \simeq 0.3$, there is a region where there are two singlet bound states. For smaller t/J and $J/J_\perp > 0$, there is a region where there are more than two singlet bound states, and in this region, the number of bound states increases as $J/J_\perp$ increases.

Fig. 14 shows the diagram for the number of triplet ($S = 1$) bound states. For $t/J \gtrsim 0.5$, there is one triplet bound state, while elsewhere no triplet bound state ex-

ists, except in a region at very small t/J.

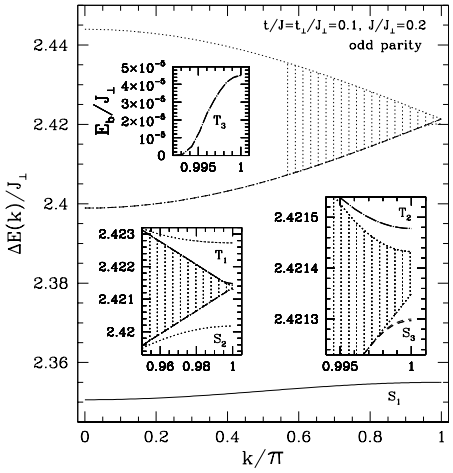

FIG. 15: The excitation spectrum in the odd parity channel at $t/J = t_\perp/J_\perp = 0.1$ and $J/J_\perp = 0.2$. Beside the two-particle continuum (gray shaded), there are three singlet bound states (S_1, S_2 and S_3) below the continuum, and three triplet antibound states (T_1, T_2 and T_3) above the continuum. Two lower insets enlarge the region near $k = \pi$ to show S_2, S_3, T_1 and T_2 below/above the continuum, but the antibound state T_3 is still indistinguishable. To see T_3, we plot the antibinding energy versus k/π, as the top inset.

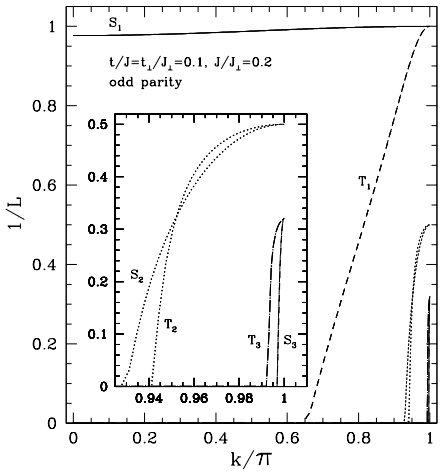

FIG. 16: The inverse of the coherence length $1/L$ versus momentum k for three singlet (S_1, S_2 and S_3), and three triplet (T_1, T_2 and T_3) antibound states for the odd parity channel at $t/J = t_\perp/J_\perp = 0.1$ and $J/J_\perp = 0.2$. The inset enlarges the region near $k = \pi$.

If we take the values $t/J = t_\perp/J_\perp = 0.1$ and $J/J_\perp = 0.2$, the two-particle excitation spectrum and the inverse of the coherence length $1/L$ versus momentum k are shown in Figs. 15 and 16. There are three singlet bound states (S_1, S_2 and S_3) below the continuum, and three triplet antibound states (T_1, T_2 and T_3) above the continuum. The singlet bound state S_1 exists for the whole range of momenta (its coherence length L is finite also for the whole range of momenta), while other bound/antibound states exist only in a limited range of momenta near $k = \pi$. At $k = \pi$, the coherence length L for S_1 and T_1 is 1, for S_2 and T_2 it is about 2, while S_3 and T_3 have coherence length L about 3. This means that the formation of bound/antibound states S_1, T_1 , S_2, T_2, S_3 and T_3 is largely due to the interaction of two antibonding rungs separated by distances 1, 1, 2, 2, 3, and 3 respectively.

If we fix the values $t/J = t_\perp/J_\perp = 0.1$ and $k = \pi$, the binding/antibinding energies E_b and the inverse of the coherence length $1/L$ versus $J/J_\perp$ are shown in Figs. 17 and 18. One can see that at the small J limit, we have two singlet bound states S_1 and S_2 (with coherence lengths 1 and 2, respectively), and two triplet antibound states T_1 and T_2 (with coherence lengths 1 and 2, respectively). As J increases, more and more singlet bound state and triplet antibound states turn up, and in our calculations, we find that states S_3, S_4, and T_3 appear at $J/J_\perp$ about 0.05, 0.12, and 0.07 respectively, while S_2, S_3, S_4, and T_1 disappear at $J/J_\perp$ about 0.32, 0.29, 0.13 and 0.46, respectively. Thus state S_4 pops out below the continuum only very briefly. The threshold index for the binding energy of S_2 and T_1 is about 1, rather than 2, as found by Dlog Padé approximants to the series.

For larger hopping terms $t/J = t_\perp/J_\perp = 1$ and $J/J_\perp = 0.2$, the two-particle excitation spectrum and the inverse of the coherence length $1/L$ versus momentum k are shown in Fig. 19. Now there is one singlet bound state S_1 and one triplet bound state (T_1) below the continuum, but no antibound state. Both S_1 and T_1 exist only in a limited range of momenta near $k = \pi$, and their coherence lengths L at $k = \pi$ are about 1.

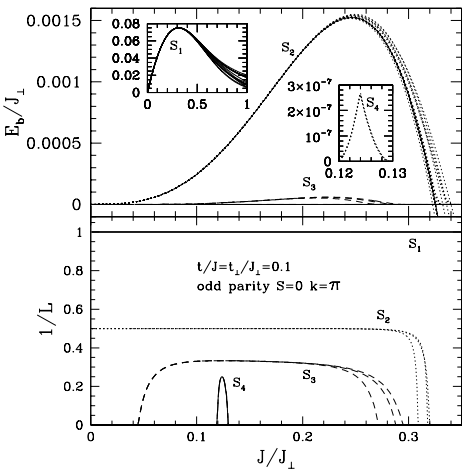

FIG. 17: The binding energy E_b and the inverse of the coherence length $1/L$ versus $J/J_\perp$ for singlet bound states in the odd parity channel at $t/J = t_\perp/J_\perp = 0.1$ and $k = \pi$. For the binding energy of S_1 and S_2, the results of several different integrated differential approximants to the series are shown, while for other curves, the results of the three highest orders are plotted.

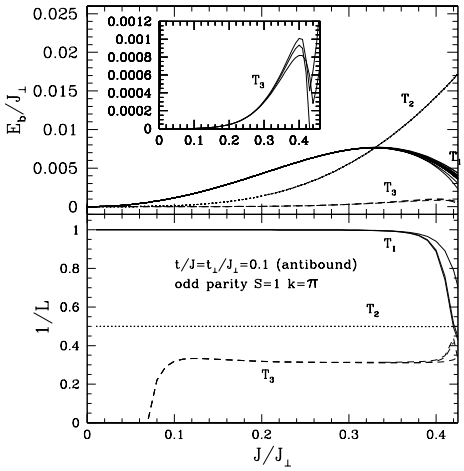

FIG. 18: The antibinding energy E_b and the inverse of the coherence length $1/L$ versus $J/J_\perp$ for triplet antibound states in the odd parity channel with $t/J = t_\perp/J_\perp = 0.1$ and $k = \pi$. For the antibinding energy of T_1 and T_2, the results of several different integrated differential approximants to the series are shown, while for other curves, the results of the three highest orders are plotted.

If we fix the values $t/J = t_\perp/J_\perp = 1$ and $k = \pi$, the binding energies E_b and the inverse of the coherence length $1/L$ versus $J/J_\perp$ are shown in Fig. 20. The singlet bound state S_1 and the triplet bound state T_1 exist as long as $J \neq 0$, but no more new bound/antibound states appear as J increases.

IV. FOUR-HOLE BOUND STATES AND PHASE SEPARATION

Among nine rung eigenstates for the unperturbed Hamiltonian H_0 on each rung, there is one state of a two-hole pair with eigenenergy 0. In this section, we discuss bound states of 2 two-hole pair excitations, corresponding to the half filled system doped with 4 holes.

As for the case of 2-hole bound states, the number of bound states and antibound states depends on $J/J_\perp$ and $t/J(= t_\perp/J_\perp)$. Fig. 21 shows the number of singlet ($S = 0$) bound states in various regions of parameter space. For large t/J ($t/J \gtrsim 0.3$) and large $J/J_\perp$, there is only one singlet bound state, while elsewhere there are two singlet bound states, except for a peculiar very narrow region (given by the bold solid line) where there is only one bound state, and a small region at low t/J (labelled by > 2) where there are more than two bound states.

If we take the values $t/J = t_\perp/J_\perp = 0.1$ and $J/J_\perp = 0.15$ (we take $J/J_\perp = 0.15$, rather than $J/J_\perp = 0.2$ as before, because at $J/J_\perp = 0.2$ we have only one bound state), the two-particle excitation spectrum and the inverse of the coherence length $1/L$ versus momentum k are shown in Figs. 22 and 23. There are two singlet bound states (S_1 and S_2) below the continuum. The singlet bound state S_1 exists for the whole range of momenta (its coherence length L is finite also for the whole range of momenta), while bound state S_2 exists only in a limited range of momenta near $k = \pi$. The coherence length L for S_1 is 1, while the coherence length L for S_2 at $k = \pi$ is about 2. This means that the formation of bound states S_1 and S_2 is largely due to the interaction

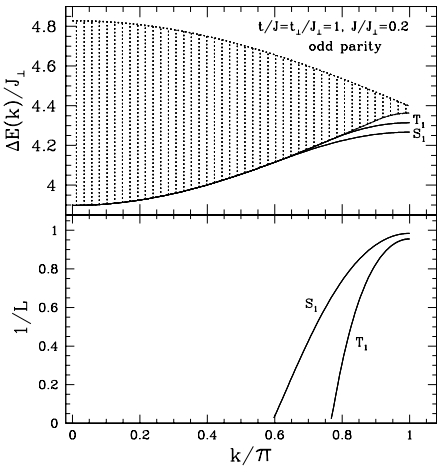

FIG. 19: The excitation spectrum and the inverse of the coherence length $1/L$ in the odd parity channel at $t/J = t_\perp/J_\perp = 1$ and $J/J_\perp = 0.2$. Beside the two-particle continuum (gray shaded), there are one singlet (S_1) and one triplet bound state (T_1) below the continuum.

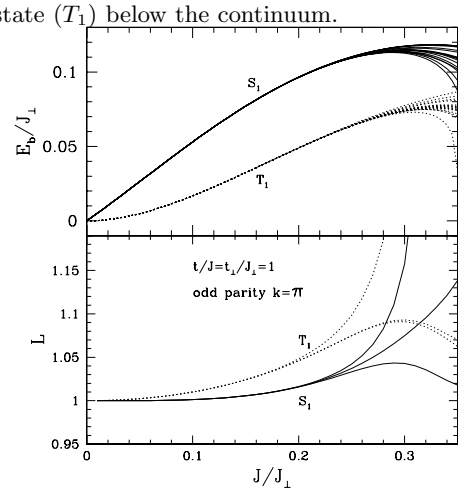

FIG. 20: The binding energy E_b and the inverse of the coherence length $1/L$ versus $J/J_\perp$ for singlet and triplet bound state in the odd parity channel at $t/J = t_\perp/J_\perp = 1$ and $k = \pi$. For the binding energy, the results of several different integrated differential approximants to the series are shown, while for the coherence length, the results of the three highest orders are plotted.

of two hole-pair rungs separated by 0 and 1 singlet rung, respectively.

If we fix the values $t/J = t_\perp/J_\perp = 0.1$ and $k = \pi$, the binding/antibinding energies E_b and the inverse of the coherence length $1/L$ versus $J/J_\perp$ are shown in Fig. 24. One can see that in the small J limit, we have two singlet bound states S_1 and S_2 (with coherence length being 1 and 2, respectively). As J increases, S_2 disappears at $J/J_\perp \simeq 0.193$, while a new antibound state S_3 and a new bound state S_4 appear at $J/J_\perp \simeq 0.205$ and 0.235, (coherence length at larger J being 2 and 3), respectively. This interval corresponds to the peculiar region given by the bold line in Fig. 21. The threshold index as the binding energy of S_2 disappears appears to be about 1 ,

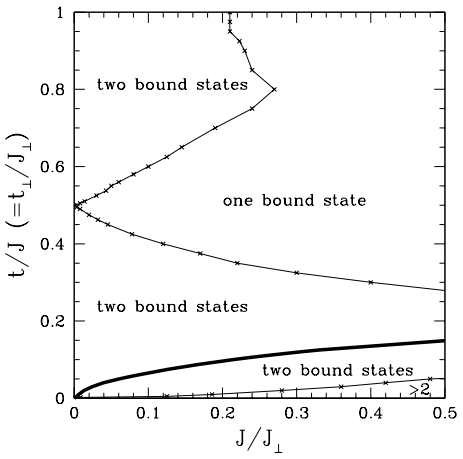

FIG. 21: The number of singlet 4-hole bound states in the plane of $t/J(= t_\perp/J_\perp)$ and $J/J_\perp$. Note that the bold solid line is the region where there is only one bound state, whereas > 2 is the region that there are more than 2 bound states.

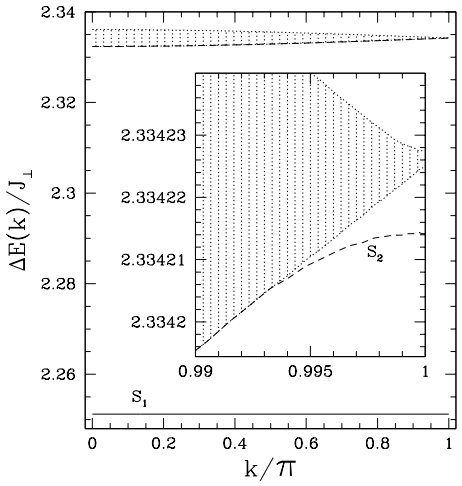

FIG. 22: The excitation spectrum for 4-hole bound states at $t/J = t_\perp/J_\perp = 0.1$ and $J/J_\perp = 0.15$. Beside the two-particle continuum (gray shaded), there are two singlet bound states (S_1 and S_2) below the continuum. The inset enlarges the region near $k = \pi$ to show S_2 below the continuum.

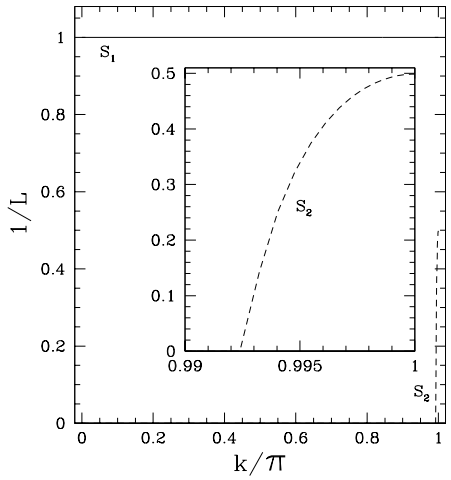

FIG. 23: The inverse of the coherence length $1/L$ versus momentum k for two singlet (S_1 and S_2) 4-hole bound states at $t/J = t_\perp/J_\perp = 0.1$ and $J/J_\perp = 0.15$. The inset enlarges the region near $k = \pi$.

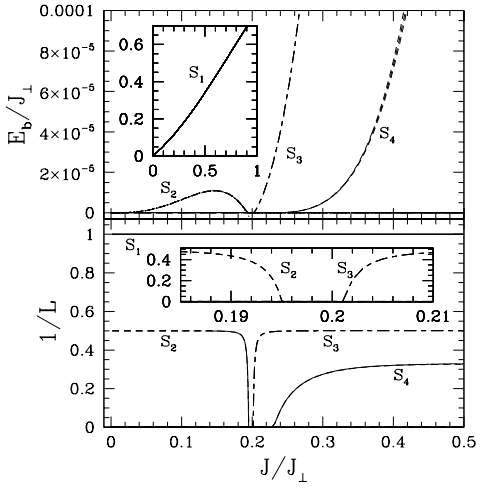

FIG. 24: The binding energy E_b and the inverse of the coherence length $1/L$ versus $J/J_\perp$ for singlet 4-hole bound/antibound states at $t/J = t_\perp/J_\perp = 0.1$ and $k = \pi$. For the binding energy of S_1 and S_2, the results of several different integrated differential approximants to the series are shown, while for other curves, the results of the three highest orders are plotted.

rather than 2. Estimates for the threshold point and index from the $[n/m]$ Dlog Padé approximants to the series for the binding energy are given in Table III. We cannot calculate a series directly for the coherence length, but from our numerical calculations, the threshold behaviour for the coherence length of S_2 is also unlikely to be the standard $L \propto (x - x_c)^{-1}$, but seems to be a weaker divergence. The dynamical reason for this unusual threshold behaviour is unclear[33]. Note that even in this case, the threshold behaviour as a function of momentum still retains the form: $E_b \propto (k - k_c)^2$, $L \propto (k - k_c)^{-1}$.

For larger hopping terms $t/J = t_\perp/J_\perp = 1$ and $J/J_\perp = 0.15$, the two-particle excitation spectrum and the inverse of the coherence length $1/L$ versus momentum k are shown in Figs. 25 and 26. Again there are two singlet bound states S_1 and S_2 below the continuum, but no antibound state. The singlet bound state S_1 exists for the whole range of momenta (its coherence length L is about 1 also for the whole range of momenta), while bound state S_2 exists only in a limited range of momenta near $k = \pi$ (its coherence length L is about 2 at $k = \pi$).

If we fix the values $t/J = t_\perp/J_\perp = 1$ and $k = \pi$, the binding energies E_b and the inverse of the coherence length $1/L$ versus $J/J_\perp$ are shown in Fig. 27. The two

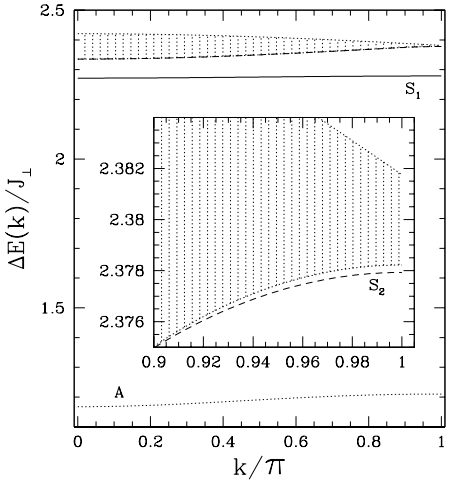

FIG. 25: The excitation spectrum for 4-holes bound state at $t/J = t_\perp/J_\perp = 1$ and $J/J_\perp = 0.15$. Beside the two-particle continuum (gray shaded), there are two singlet (S_1 and S_2) below the continuum. Curve A is the dispersion of the two-holes sitting in the same rung.

singlet bound states S_1 and S_2 exist as long as $J \neq 0$, but as J increases, no more new bound/antibound states appear, but S_2 disappears at $J/J_\perp \simeq 0.22$.

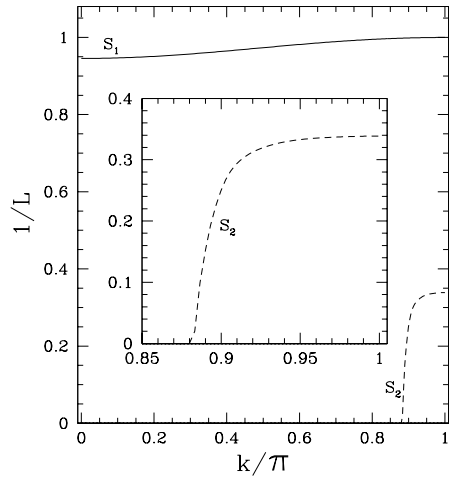

FIG. 26: The inverse of the coherence length $1/L$ versus momentum k for two singlet (S_1 and S_2) 4-holes bound states at $t/J = t_\perp/J_\perp = 1$ and $J/J_\perp = 0.15$. The inset enlarges the region near $k = \pi$.

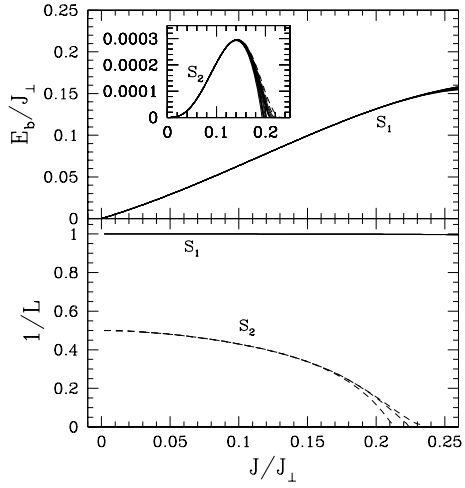

FIG. 27: The binding energy E_b and the inverse of the coherence length $1/L$ versus $J/J_\perp$ for two singlet 4-holes bound states at $t/J = t_\perp/J_\perp = 1$ and $k = \pi$. For the binding energy, the results of several different integrated differential approximants to the series are shown, while for the coherence length, the results of the three highest orders are plotted.

The compressibility κ is given by

$$\kappa^{-1} = \rho^2 \frac{\partial^2 \epsilon}{\partial \rho^2} \tag{9}$$

where $\epsilon(\rho)$ is the energy density of the ladder with hole density ρ. For a finite system at half-filling this can be replaced by the discrete version

$$\kappa^{-1} = (L/2)[E_0(\frac{1}{2} \text{ filled}) - 2E_0(2 \text{ holes}) + E_0(4 \text{ holes})]$$
$$= (L/2)[\Delta E_0(4 \text{ holes}) - 2\Delta E_0(2 \text{ holes})] \tag{10}$$

where for a ladder of L rungs, ΔE_0 is the minimum energy gap for 2 or 4 holes, and this minimum energy gap is at momentum $k = 0$. Now if the 2-hole pair on a single rung is the lowest-energy state in the 2-hole sector, and at momentum $k = 0$ two 2-hole rungs form a bound state in the 4-hole sector, then it immediately follows that κ^{-1} as defined by Eq. 10 diverges to negative infinity as $L \to \infty$, signalling *phase separation*. Comparing Figures 21 and 12, we see that these conditions apply, and phase separation occurs, over the whole of the lower region of Figure 12.

Outside this region, we know the energy of the lowest state in the 2-hole sector, consisting of a bound pair of holes on different rungs (denoted S_1, previously). The bound state of two 2-hole rungs may not be the lowest-energy state in the 4-hole sector; but at least it allows us to place an upper limit on κ^{-1} as defined by Eq. 10. We find that this limit is negative, and therefore phase separation must occur, for $t/J(= t_\perp/J_\perp)$ anywhere below a value about 0.5, independent of $J/J_\perp$ - although due to numerical uncertainty, this estimate cannot be made very precise. This is in good agreement with previous estimates: Rommer *et al.*[21], for instance, find the phase separation boundary at half-filling to lie at $J/t = 2.156(2)$, or $t/J = 0.464$, from a density matrix renormalization group calculation for the isotropic ladder.

V. DISCUSSION AND SUMMARY

We have used linked-cluster series expansion methods[5] to study 2-hole bound states in the $t-J$ ladder. The series only converge well for $J/J_\perp \lesssim 0.5$, so we are unable to say very much about the isotropic case $J = J_\perp$. Dispersion relations and coherence lengths have been computed for various bound states in even- and odd- parity channels. A rich spectrum of these states has emerged.

The most striking feature of the results is the appearance of multiple bound states in both singlet $S = 0$

and triplet $S = 1$ channels as the ratio $t/J(= t_\perp/J_\perp)$ goes to zero for finite $J/J_\perp$. What is the cause of this phenomenon? The limit $t/J \to 0$ corresponds to the antiferromagnetic Heisenberg ladder with 2 static holes. Beyond states S_0 and S_1, all the multiple bound states $(S_2, \cdots)$ only emerge near $k = \pi$, and all have small binding energies: their dynamical significance is unclear.

Another interesting feature is that in the even-parity channel, at least, all the triplet $S = 1$ bound states seem to disappear as the isotropic limit $J/J_\perp \to 1$ is approached, leaving only singlet $S = 0$ bound states. Other studies[28] have found the same thing. We have no explanation for this phenomenon, either.

Jurecka and Brenig[28] have put forward a semi-analytic theory of 2-hole excitations in the $t - J$ ladder, based on the dimerized rung picture, with elementary excitations consisting of the single-hole pseudofermion excitations and the 2-hole singlet excitation on a single rung, plus singlet and triplet "bond boson" operators for spin excitations, and applying a linearized Holstein-Primakoff approach. They present a spectrum showing only one $S = 0$ and one $S = 1$ bound state, at couplings which are not accessible to our series approach.

The question of phase separation has also been explored. We have been able to calculate the energy of a 4-hole state consisting of two 2-hole rungs, giving an upper limit on the inverse compressibility at half-filling. Hence it can be shown that phase separation occurs for $t/J \lesssim 0.5$, in agreement with other studies[21]. Most of the interesting spectral features occur, unfortunately, in the phase separated region.

We have also explored the threshold behaviour of these bound/antibound states as they emerge from the continuum. As a function of momentum, the binding energy near threshold behaves as $E_b \propto (k - k_c)^2$, and the coherence length as $L \propto (k - k_c)^{-1}$ in every case we have studied so far. This appears to be standard: for instance, a model of the bound states of two magnons by Sushkov and Kotov[7] gives this behaviour. As a function of coupling $x = J/J_\perp$, the typical threshold behaviour is similar, $E_b \propto (x - x_c)^2$, $L \propto (x - x_c)^{-1}$. We have found examples, however, where the binding energy appears to behave as $E_b \propto (x - x_c)$, see Sect. IIIB and IV.

In conclusion, then, we have discovered a rich and diverse spectrum of 2-hole bound states in the $t - J$ ladder at half-filling. They exhibit a number of interesting feature which call for a theoretical explanation; and fitting these data will provide a stringent test of any theoretical model of the system. It would also be interesting if it were possible to test these features experimentally.

Acknowledgments

We are grateful to Prof. Jaan Oitmaa and Oleg Sushkov for useful discussions. This work forms part of a research project supported by a grant from the Australian Research Council. The computations have been performed on an AlphaServer SC computer. We are grateful for the computing resources provided by the Australian Partnership for Advanced Computing (APAC) National Facility.

* w.zheng@unsw.edu.au; http://www.phys.unsw.edu.au/~zwh

† c.hamer@unsw.edu.au

[1] E. Dagotto and T.M. Rice, Science **271**, 618(1996).

[2] T.M. Rice, Z. Phys. B**103**, 165(1997).

[3] M. Azuma, Z. Heroi, M. Takano, K. Ishida and Y. Kitaoka, Phys. Rev. Lett. **73**, 3463(1994).

[4] M. Uehara *et al.* J. Phys. Soc. Jpn **65**, 2764(1996).

[5] S. Trebst, H. Monien, C. J. Hamer, W. H. Zheng and R. R. P. Singh, Phys. Rev. Lett. **85**, 4373(2000).

[6] V.N. Kotov, O. Sushkov, W. Zheng and J. Oitmaa, Phys. Rev. Lett. **80**, 5790(1998).

[7] O.P. Sushkov and V.N. Kotov, Phys. Rev. Lett. **81**, 1941(1998).

[8] S. Sachdev and R. Bhalt, Phys. Rev. B **41**, 9323(1990).

[9] S. Gopalan, T.M. Rice and M. Sigrist, Phys. Rev. B**49**, 8901(1994).

[10] K. Damle and S. Sachdev, Phys. Rev. B **57**, 8307 (1998).

[11] E. Dagotto, J. Riera and D.J. Sealapino, Phys. Rev. B **45**, 5744(1992).

[12] D. Poilblanc, D.J. Scalapino and W. Hanke, Phys. Rev. B **52**, 6796(1995).

[13] M. Troyer, H. Tsunetsugu and T.M. Rice, Phys. Rev. B **53**, 251(1996).

[14] C.A. Hayward, D. Poiblanc, Phys. Rev. B**53**, 11721(1996).

[15] C.A. Hayward, D. Poiblanc, and D.J. Scalapino, Phys. Rev. B**53**, R8863(1996).

[16] T.F.A. Müller and T.M. Rice, Phys. Rev. B **58**, 3425(1998).

[17] J. Riera, D. Poilblanc and E. Dagotto, Eur. Phys. J B **7**, 53(1999).

[18] S.R. White and D.J. Scalapino, Phys. Rev. B **55**, 6504(1997).

[19] G. Sierra, M.A. Martin-Delgado, J. Dukelsky, S.R. White, and D.J. Scalapino, Phys. Rev. B **57**, 11666(1998).

[20] C. Gazza, G.B. Martins, J. Riera and E. Dagotto, Phys. Rev. B**59**, 709(1999).

[21] S. Rommer, S.R. White and D.J. Scalapino, Phys. Rev. B**61**, 13424(2000).

[22] M. Brunner, S. Capponi, J.F. Assaad and A. Muramatsu, Phys. Rev. B**63**, 180511(2001).

[23] J. Oitmaa, C.J. Hamer and W.H. Zheng, Phys. Rev. B **60**, 16364(1999).

[24] W.H. Zheng, C.J. Hamer, J. Oitmaa, and R.R.P. Singh, cond-mat/0112371.

[25] M. Sigrist, T.M. Rice and F.C. Zhang, Phys. Rev. B **49**, 12058(1994).

[26] Y.L. Lee, Y.W. Lee, C.Y. Mou and Z.Y. Weng, preprint cond-mat/9903059.

[27] O.P. Sushkov, Phys. Rev. B **60**, 3289(1999).

[28] C. Jurecka and W. Brenig, cond-mat/0107365.

[29] W.H. Zheng, C.J. Hamer, R.R.P. Singh, S. Trebst, and H. Monien, Phys. Rev. B 63, 144410 (2001).

[30] G. S. Uhrig and F. Schönfeld, M. Laukamp and E. Dagotto, Eur. Phys. J. B **7**, 67 (1999).

[31] E.S. Sørensen, I. Affleck, D. Augier and D. Poilblanc, Phys. Rev. B**58**, R14701 (1998).

[32] A.J. Guttmann, in "Phase Transitions and Critical Phenomena", Vol. 13 ed. C. Domb and J. Lebowitz (New York, Academic, 1989).

[33] Prof. O. Sushkov has suggested that it may correspond to a "d-wave" rather than "s-wave" threshold.

TABLE I: The nine rung states and their energies at $t = J = 0$.

No.	Eigenstate	Eigenvalue	Name
1	$\frac{1}{\sqrt{2}}(\|\uparrow\downarrow\rangle - \|\downarrow\uparrow\rangle)$	$-J_\perp$	singlet
2	$\|\downarrow\downarrow\rangle$	0	triplet ($S^z_{\rm tot} = -1$)
3	$\frac{1}{\sqrt{2}}(\|\uparrow\downarrow\rangle + \|\downarrow\uparrow\rangle)$	0	triplet ($S^z_{\rm tot} = 0$)
4	$\|\uparrow\uparrow\rangle$	0	triplet ($S^z_{\rm tot} = 1$)
5	$\|\,00\rangle$	0	hole-pair singlet
6	$\frac{1}{\sqrt{2}}(\|\,0\downarrow\rangle + \|\downarrow 0\rangle)$	$-t_\perp$	electron-hole bonding ($S^z_{\rm tot} = -\frac{1}{2}$)
7	$\frac{1}{\sqrt{2}}(\|\,0\uparrow\rangle + \|\uparrow 0\rangle)$	$-t_\perp$	electron-hole bonding ($S^z_{\rm tot} = \frac{1}{2}$)
8	$\frac{1}{\sqrt{2}}(\|\,0\downarrow\rangle - \|\downarrow 0\rangle)$	$t_\perp$	electron-hole antibonding ($S^z_{\rm tot} = -\frac{1}{2}$)
9	$\frac{1}{\sqrt{2}}(\|\,0\uparrow\rangle - \|\uparrow 0\rangle)$	$t_\perp$	electron-hole antibonding ($S^z_{\rm tot} = \frac{1}{2}$)

TABLE II: Series coefficients for dimer expansions for the energy gap $E/J_\perp$ of two singlet bound states (S_1 and S_2), one triplet bound state (T_1), and the lower edge of the continuum (C_l) at $k = \pi$, for the bound states of two even parity holes of the $t - J$ ladder with $y_1 = y_2 = 0.1$. Nonzero coefficients x^n up to order $n = 11$ are listed.

n	$E_{S_1}/J_\perp$ for S_1	$E_{S_2}/J_\perp$ for S_2	$E_{T_1}/J_\perp$ for T_1	$E_{C_l}/J_\perp$ for C_l
0	1.8000000000	1.8000000000	1.8000000000	1.8000000000
1	$5.0000000000\times10^{-1}$	1.0000000000	1.0000000000	1.0000000000
2	$2.2500000000\times10^{-1}$	$8.5000000000\times10^{-1}$	$8.0000000000\times10^{-1}$	$8.5000000000\times10^{-1}$
3	$4.2708333333\times10^{-1}$	$3.2811666667\times10^{-1}$	$3.8020833333\times10^{-1}$	$4.5625000000\times10^{-1}$
4	$9.8972656250\times10^{-1}$	$-5.0189024889\times10^{-1}$	$-2.1309606481\times10^{-1}$	$-2.0194444444\times10^{-1}$
5	$-1.4465469473\times10^{-1}$	-1.0020098268	$-6.5367901837\times10^{-1}$	$-7.4625737847\times10^{-1}$
6	-3.6759280211	$-5.2752447741\times10^{-1}$	$-5.1516620601\times10^{-1}$	$-5.7308628683\times10^{-1}$
7	-1.8432595464	$9.3228166551\times10^{-1}$	$2.9350608457\times10^{-1}$	$4.7837543431\times10^{-1}$
8	1.2540109894×10^{1}	2.4273057426	1.1202826230	1.5454790111
9	1.1255237404×10^{1}	2.2797858202	$8.6634384749\times10^{-1}$	1.0984536226
10	$-4.7671925391\times10^{1}$	$-5.2477491651\times10^{-1}$	$-8.6710572784\times10^{-1}$	-1.4110630505
11	$-5.6591915055\times10^{1}$	-4.6480530617	-2.6386765415	-3.8611918629

TABLE III: $[n/m]$ D log Padé approximants to the series for bining energy $E_b/J_\perp$ at $k = \pi$ of singlet bound state S_2 of 4-holes at $t/J = t_\perp/J_\perp = 0.1$. An asterisk denotes a defective approximant.

n	$[(n-2)/n]$	$[(n-1)/n]$	$[n/n]$	$[(n+1)/n]$	$[(n+2)/n]$
	pole (residue)	pole (residue)	pole (residue)	pole (residue)	pole (residue)
n= 1			0.19966(1.1704)	0.19987(1.1741)	0.19391(1.0401)
n= 2		0.19987 (1.1741)	0.19967(1.1705)	0.19194(0.9851)	0.19250(1.0032)
n= 3	0.19415(1.0485)*	0.19255 (1.0055)	0.19265(1.0088)	0.19272(1.0117)	0.19280(1.0154)
n= 4	0.19264(1.0086)	0.19288 (1.0202)*	0.19296(1.0259)*	0.19171(1.0808)*	
n= 5	0.19295(1.0259)*	0.19285 (1.0185)*			